ACTA ONCOLOGICA
2023, VOL. 62, NO. 11, 1566–1573
https://doi.org/10.1080/0284186X.2023.2246641

Taylor & Francis
Taylor & Francis Group

ORIGINAL ARTICLE



# An experimental setup for proton irradiation of a murine leg model for radiobiological studies

Cathrine Bang Overgaard[a,b], Fardous Reaz[a,b,c], Mateusz Sitarz[b,c], Per Poulsen[b,c], Jens Overgaard[a,b], Niels Bassler[a,b,c], Cai Grau[b,c] and Brita Singers Sørensen[a,b,c]

[a]Department of Experimental Clinical Oncology, Aarhus University Hospital, Denmark; [b]Department of Clinical Medicine, Aarhus University, Aarhus, Denmark; [c]Danish Centre for Particle Therapy, Aarhus University Hospital, Denmark

**ABSTRACT**

**Background:** The purpose of this study was to introduce an experimental radiobiological setup used for *in vivo* irradiation of a mouse leg target in multiple positions along a proton beam path to investigate normal tissue- and tumor models with varying linear energy transfer (LET). We describe the dosimetric characterizations and an acute- and late-effect assay for normal tissue damage.

**Methods:** The experimental setup consists of a water phantom that allows the right hind leg of three to five mice to be irradiated at the same time. Absolute dosimetry using a thimble (Semiflex) and a plane parallel (Advanced Markus) ionization chamber and Monte Carlo simulations using Geant4 and SHIELD-HIT12A were applied for dosimetric validation of positioning along the spread-out Bragg peak (SOBP) and at the distal edge and dose fall-off. The mice were irradiated in the center of the SOBP delivered by a pencil beam scanning system. The SOBP was 2.8 cm wide, centered at 6.9 cm depth, with planned physical single doses from 22 to 46 Gy. The biological endpoint was acute skin damage and radiation-induced late damage (RILD) assessed in the mouse leg.

**Results:** The dose–response curves illustrate the percentage of mice exhibiting acute skin damage, and at a later point, RILD as a function of physical doses (Gy). Each dose–response curve represents a specific severity score of each assay, demonstrating a higher ED50 (50% responders) as the score increases. Moreover, the results reveal the reversible nature of acute skin damage as a function of time and the irreversible nature of RILD as time progresses.

**Conclusions:** We want to encourage researchers to report all experimental details of their radiobiological setups, including experimental protocols and model descriptions, to facilitate transparency and reproducibility. Based on this study, more experiments are being performed to explore all possibilities this radiobiological experimental setup permits.

**ARTICLE HISTORY**
Received 14 June 2023
Accepted 3 August 2023

**KEYWORDS**
Radiobiology; experimental setup; dosimetry; in vivo; acute skin damage; radiation-induced late damage (RILD); linear energy transfer (LET)

## Introduction

The number of proton radiotherapy facilities worldwide is increasing because of protons' favorable dose-depth distribution with tissue-sparing properties. The biological translation from conventional radiotherapy to protons has been extensively researched *in vitro* [1–3]. The connecting link between *in vivo* data and *in vitro* data, however, is missing within certain areas of proton radiobiology: 1) quantification of the variable relative biological effectiveness (RBE) between X-rays and protons [2–5], 2) the increased biological effect at the distal end of the proton track in a spread-out Bragg peak (SOBP) [6–8], 3) the effects of proton FLASH on normal tissues and tumor models [9,10], 4) spatially fractionated GRID proton therapy [11], and 5) the synergistic effects of radiotherapy in combination with other cancer treatments such as immunotherapy [12] and hyperthermia [13]. These are all examples of topics in need of biological characterization *in vivo*.

To increase the understanding of radiobiology and harvest the full potential of protons, reliable and thoroughly tested setups for radiobiological experiments are important. Highly specialized qualitative experimental setups endorse treatment planning systems and image guidance to improve dosimetry and geometric accuracy in radiotherapy [14,15]. One laboratory team demonstrated an impressive novel experimental design for proton irradiation of small sub-volumes in the mouse brain [16,17]. They can obtain highly accurate targeting expressed by DNA double-strand breaks along the beam SOBP. Another team [18] used an experimental setup for intestinal crypt regeneration where whole-body irradiation was applied. A panel of different radiobiological setups is crucial to investigate and answering different research questions. However, in general, many experimental setups often do not

CONTACT Cathrine Bang Overgaard Cathrine@oncology.au.dk Department of Experimental Clinical Oncology, Aarhus University Hospital, Denmark
Supplemental data for this article can be accessed online at https://doi.org/10.1080/0284186X.2023.2246641.

possess the cohort size capacity to quantitatively establish a certain biological effect or dose–response relationship that can be converted into fundamental clinical assessments. In 1980, Overgaard et al. [19] described the experimental setup for the first time that, at that time, allowed isolated photon irradiation of mice extremities. Originally, the setup was developed for hyperthermia, but the homogenous conditions offered by a water phantom made the effect of combining hyperthermia and radiation promising.

The documentation of experimental small animal radiation setups is in demand of standard reporting procedures, including dosimetry and specific details of experiment execution [14,20–22]. Poor reporting of experimental methodology endangers the reproducibility and credibility of the test results. Bearing in mind the increasing demand for reporting experimental details regarding radiation setups and dosimetry, we grasp the opportunity to present our mice experimental setup for particles that are easily navigated and allow investigation of a variety of biological effects after irradiation. It enables the examination of biological effects following irradiation of mice legs at different positions of the SOBP, including proximal, center, and distal edge positions. This setup is highly suitable for RBE studies, the biological effects of clinically relevant fractionation schemes, GRID proton therapy research, and the FLASH effect in tumors and normal tissues as it quantifies endpoints that are locally and controlled positioned on mice extremities.

This report aims to describe one of the experimental setups that we use for radiobiological *in vivo* research of normal tissue damage and tumor response. Furthermore, it aims to describe the acute- and late-toxicity assays we use for normal tissue damage analysis after irradiation.

## Materials and methods

### *Experimental setup*

All proton irradiations were performed at the experimental proton beamline at the Danish Center for Particle Therapy (DCPT) at Aarhus University Hospital, Denmark, using a horizontal proton scanning pencil beam (ProBeam, Varian, a Siemens Healthineers Company, Palo Alto, CA, USA). Beam energies up to 250 MeV were provided by an isochronous cyclotron. For the results presented in this paper, a proton field of 120.4 mm width and 34.0 mm height in the isocenter plane was applied. It was formed by eight energy layers ranging from 84.38 to 106.48 MeV to cover a planning target volume (PTV) of $10 \times 3 \times 3\,cm^3$ (i.e., 3 cm wide and deep) that covers the targeted feet of the mice.

The ankle joint of the mice was placed in the rim of the PTV, which may have reduced the ankle joint dose. An explanation is investigated in another paper that will be published later. Nominal PTV doses ranged from 22 to 46 Gy physical doses. The entire field was typically delivered within 2–7 min.

The setup consisted of a water phantom with 1 cm acrylic glass (PMMA) walls with outer dimensions of w: 45 cm × d: 34.3 cm × h: 25 cm (Figure 1(A,B)). The phantom was developed as a particle counterpart to the reported X-ray phantom in reference [19]. The water temperature was maintained at 24–26 °C and always monitored during the experiments. The water surface measured from the phantom base was located at a height of 19 cm, whereupon a 0.5-cm thick plate of PMMA enabled the positioning of mice jigs. The PMMA plate could be exchanged into various versions and may have either three or five slots where mouse jigs could be inserted while the right hindlimb was immersed into the water through openings carved into the PMMA top plate. The PMMA top plate enables movement along the beam direction into eight different positions in 4 mm intervals covering the proximal to the distal dose fall-off of the SOBP, as illustrated in Figure 1(A,C). To have a very rigid setup with high reproducibility, much attention and care was given to the setup as the phantom was disassembled and reassembled again. Fine adjustment of depth in smaller steps than 4 mm was possibly realized by adding $<4$ mm thick PMMA spacers at the phantom entrance. The mice bodies were shielded from primary protons by brass blocks (primary shielding), which also provided a sharp cutoff dose gradient of the upper edge of the proton field. A notch carved into the primary brass shield made room for the bent mice tails and ensured minimal distance from the brass shield to the mice, as shown in Figure 1(C). Multiple brass blocks were manufactured so they could be exchanged during experiments because of induced radioactivity, which, if not mitigated, could lead to radiation protection issues. Whereas the activated phantom materials (PMMA and water) decay to acceptable levels within minutes, activated brass involved nuclides with longer half-lives. Induced radioactivity buildup is effectively avoided by recycling up to four brass collimators, depending on the delivered dose (and field size, which, however, was not varied during this work). Eventually, a cooling-down period of 10–15 min was needed post-irradiation before entering the experimental room to allow the dose rate to reach below 50 μSv/h on the phantom surface.

The entire setup was made available as a supplemental CAD file as supplemental material. In the setup configuration used in this work, the center of a 2.8-cm wide SOBP was located 6 cm from the water phantom's inner edge and annotated as "position no. 2" in Figure 1(A). A plate for three mice separated by 3.5 cm was used, and the mice were irradiated only in the center SOBP position. The range of physical doses between 22 and 46 Gy was selected based on previous data [23].

The unanesthetized mice were inserted into small jigs modified from ref [19]. The jigs used in the present pilot study were made of a hollow black tube with air holes and a supporting PMMA plate, which defined the position of the mice leg (Figure 1(D)). The leg rested on the PMMA with a backrest to avoid the mice moving their legs backward. To prevent the mice from escaping, the tail was needled through a hole in the PMMA and attached to the top of the jig with micropore tape, as visualized in Figure 1(D). The right hindlimb was then attached with a small droplet of histoacrylic glue on the inner thigh/ankle joint. While the glue dried, a piece of tape was placed tightly around the upper thigh for 3–5 min, followed by a resting period of 10 min

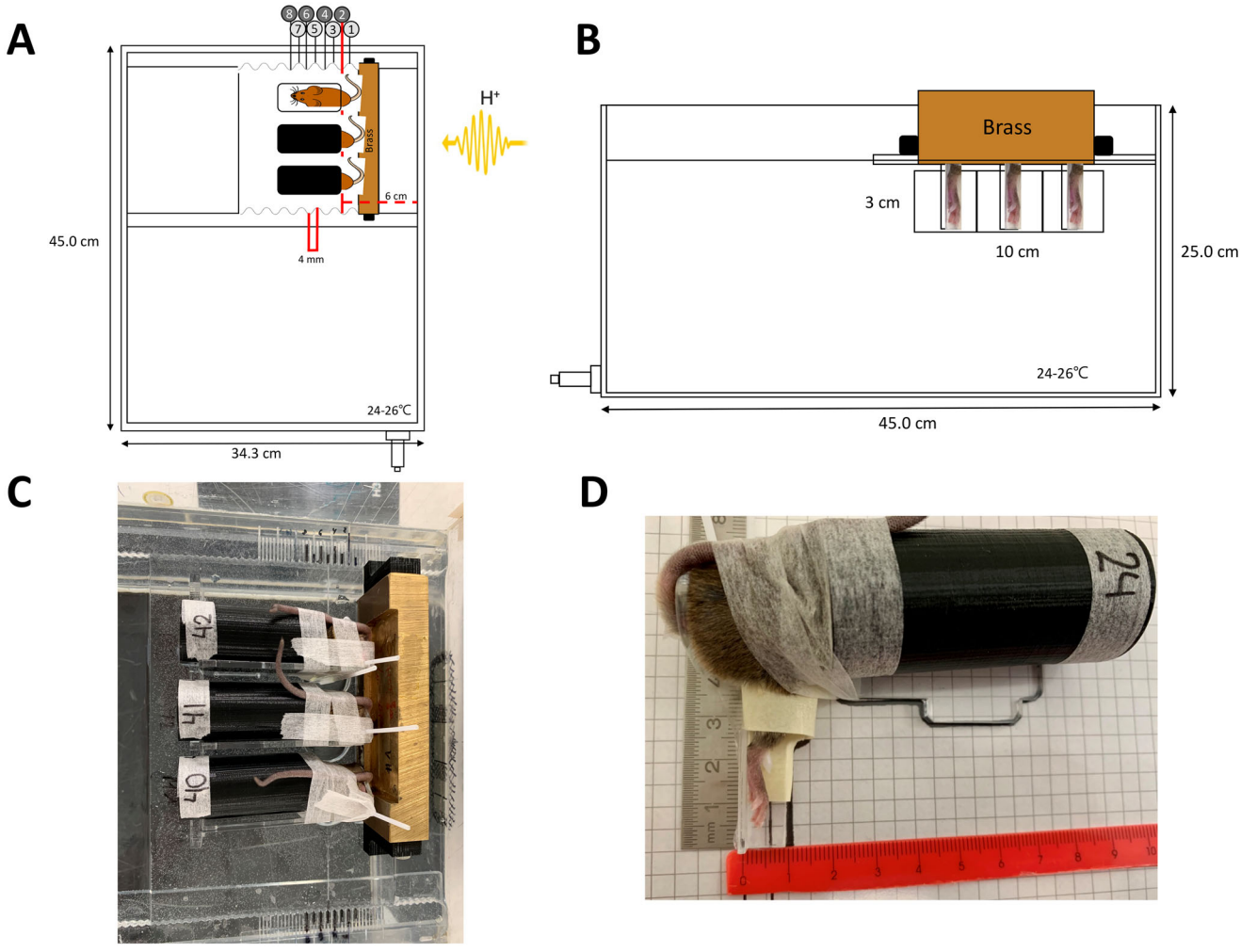


**Figure 1.** Experimental setup for a local biological response on the right hindleg of mice. Schematics of the water phantom from a top-down view (A) with three black tubes containing mice positioned on top of a movable plastic plate and from the beam direction (B) with mice feet positioned in the proton field and bodies shielded by brass. (C) Top-down view of the experimental setup with mice and brass and (D) mouse jig with mouse and glued right hindlimb.

with the tape loosened. In the case of tumor experiments, the tumor would be placed on top of the foot, where the leg would be restrained by a loose piece of tape across the upper thigh (see ref [19]). A template for leg-positioning in the jig was used to position the legs of the mice identically in the jigs. The thickness of the leg and the horizontal and vertical leg position in the jigs were noted from the rulers seen in Figure 1(D). A GoPro camera was used to video record the mice during each round of irradiation. The mice were irradiated at the same time interval of the day to avoid any circadian influence on the radiation response. At the end of all treatments, the mice were detached from the jig and released back into their respective cages to await follow-up.

### *Dosimetry*

Absolute dosimetry was performed using a thimble (PTW TM31010 Semiflex) and a plane parallel (PTW TW34045 Advanced Markus) ionization chamber (IC). The Semiflex IC was calibrated in 2022 at the National Physical Laboratory (NPL, Teddington, UK) against a primary standard, and the Adv.Markus chamber was calibrated the same year at PTW Freiburg in Germany against a secondary standard. Both were calibrated in a Co-60 reference beam. The biological experiments were performed approximately 1.5 years before the Semiflex IC calibration. The IAEA TRS-398 dosimetry protocol for proton beams was followed [24]. The Semiflex ionization chamber was inserted in a special mouse holder, with a matching PMMA cylinder for the IC at the position of a mouse leg. It was used for absolute dosimetry along the SOBP using different top plate positions and laterally using different mouse jig positions in the top plate. However, at the distal edge of the SOBP, thimble ionization chambers become less useful as the effective point of measurement cannot be assumed to be at the center of the ion chamber axis.

To resolve the exact position of the distal edge of the SOBP, a full depth-dose curve was recorded with an Advanced Markus chamber. Here, the waterproof cap was used, which adds 1.04 mm of water equivalent thickness to the measurement depth. Recombination ($k_s$) and polarity effects ($k_{pol}$) were measured and found to be negligible. kQ factors for both ICs were taken and interpolated from ref [25].

The details of Monte Carlo Simulations are described in the supplementary section.

### Animals and radiation response

This study included 160 $C_3$H/HeNRj mice of 14–16 week of age that was divided into dose groups of 5–24 animals per group. The animals were bought from Janvier Labs (France) and transported together under conditions that minimize stress during travel. Before experiments, the mice acclimatized for 4 weeks in a housing of three to four mice per cage at the animal facility at Experimental Clinical Oncology, Aarhus University Hospital. The mice were randomly divided into cages. Only females were used in the experiments to circumvent any sex differences. The daily cage temperature was set to 22–23 °C with a dark and light cycle of 12 h. There was ad libitum food and water access for all mice cages, and the mice were weighed every seventh day during the follow-up period. All experiments were performed following the Institutional and National Guidelines for Animal Welfare under license no 2017-15-0201-01218. Each cage was blindly designated a radiation dose. During the experiment and follow-up, the mice handlers were blinded to the radiation dose and the analysis score from the day before.

The endpoints used for our normal tissue damage research are acute skin damage on the feet and radiation-induced late damage (RILD) development in the ankle joint. Both categorical analysis tables are presented in Table 1.1. The acute skin damage analysis is based on a slightly modified analysis table that is originally described by Von der Maase in ref [26]. From this, the irradiated foot was visually inspected and received a skin score from 0 to 3.5 in steps of 0.5, with 3.5 as the most severe skin damage. The leg of the mice was analyzed within the same time interval (3 h) daily from day 7 to 30.

The same mice were analyzed for RILD development in a functional leg flexibility assay based on Stone in ref [27] and first modified and used in ref [28]. Here, the ability to stretch the ankle joint of the irradiated right hindleg was analyzed and handed a RILD categorical score between 0 and 4, graded in steps of 1 (see Table 1.2). Score 1 is considered mild, score 2 as medium, score 3 as severe, and score 4 as total fixation of the joint. The mice were assessed every 14th day from 9 to 53 weeks after irradiation. When graded, each mouse is fixated and placed on top of the template guideline seen in Supplementary Figure 1. The thumb is placed behind the ankle joint where the index finger gently extends/flexes the joint until natural resistance occurs. Importantly, no force is applied.

For both endpoint analyses, the left unirradiated hindlimb serves as a control together with unirradiated control mice.

### Data analysis and statistics of biological data

For statistical examination and graphical illustration of the biological data, Stata 17.0 (Stata/IC17.0, Stata Corp LP, Texas, College Station, USA) and GraphPad Prism 9.4 (GraphPad Software, LA Jolla, CA, USA) were used. Dose–response curves for the percentage of mice exhibiting an acute skin damage score (2–3.5) and an RILD score (1–4) as a function of physical dose were fitted using simple logistic regression. Each score was given a minimum of once during their follow-up. The effective dose of 50% responders (ED50) and their 95%-confidence intervals (95% CI) were extracted. The median score of acute skin damage and RILD was plotted as a function of days or weeks post-treatment.

## Results

Figure 2 shows dose–response curves for A) acute skin damage developing between 7 and 30 days post-treatment and B) RILD development after 6 months, C) 9 months, and D) 12 months post-treatment. For each assay (acute and late), the table scores are plotted to illustrate a dose–response relationship, each with a higher ED50 as the scores increase. The ED50 with their 95%CI for each score is indicated in the figures. The median acute skin damage development is plotted in Figure 3(A) as a function of the days after irradiation. The development of RILD is plotted as the median RILD score as a function of weeks in Figure 3(B). Notably, with time, the median skin score increases and reaches a plateau, followed by descending curves toward day 30. For RILD, the curves slowly increase toward the 12 months, e.g., showing an irreversible tendency. For the sake of simplicity, only representable doses are depicted in Figure 3; however, all doses are illustrated in Supplementary Figures 2(A,B).

Absolute dosimetry showed that the Semiflex ionization chamber was within 1% of the planned PTV dose. At the distal edge, the reference position indicated a shift of 1.25 mm, which

**Table 1.** Categorical analysis tables for 1) acute skin damage scoring table and 2) RILD flexibility scoring table.

1)

| Score | Criteria for acute skin damage scoring |
|---|---|
| 0.5 | Slight reddening, <25% hair loss |
| 1 | Severe reddening, swelling, 25–75% hair loss |
| 1.5 | Moist desquamation of one small area, two toes partly stuck together, >75% hair loss |
| 2 | Moist desquamation of 25% of skin area, two toes stuck together, general shape unchanged, all toes can be identified |
| 2.5 | Moist desquamation of 50% of skin area, toes stuck together, general shape changed, at least three toes can be identified |
| 3 | Moist desquamation of 75% of skin area, foot shapeless, 1 or 2 toes can be identified |
| 3.5 | Moist desquamation of the entire skin area, foot shapeless |

2)*

| Score | Criteria for fibrosis scoring |
|---|---|
| 0 | Total flexibility (100% flexibility) |
| 1 | Mildly reduced flexibility (75% flexibility) |
| 2 | Medium reduced flexibility (50% flexibility) |
| 3 | Severe reduced flexibility (25% flexibility) |
| 4 | Total fixation of joint (0% flexibility) |

*For template guideline visualization see Supplementary Figure 1.

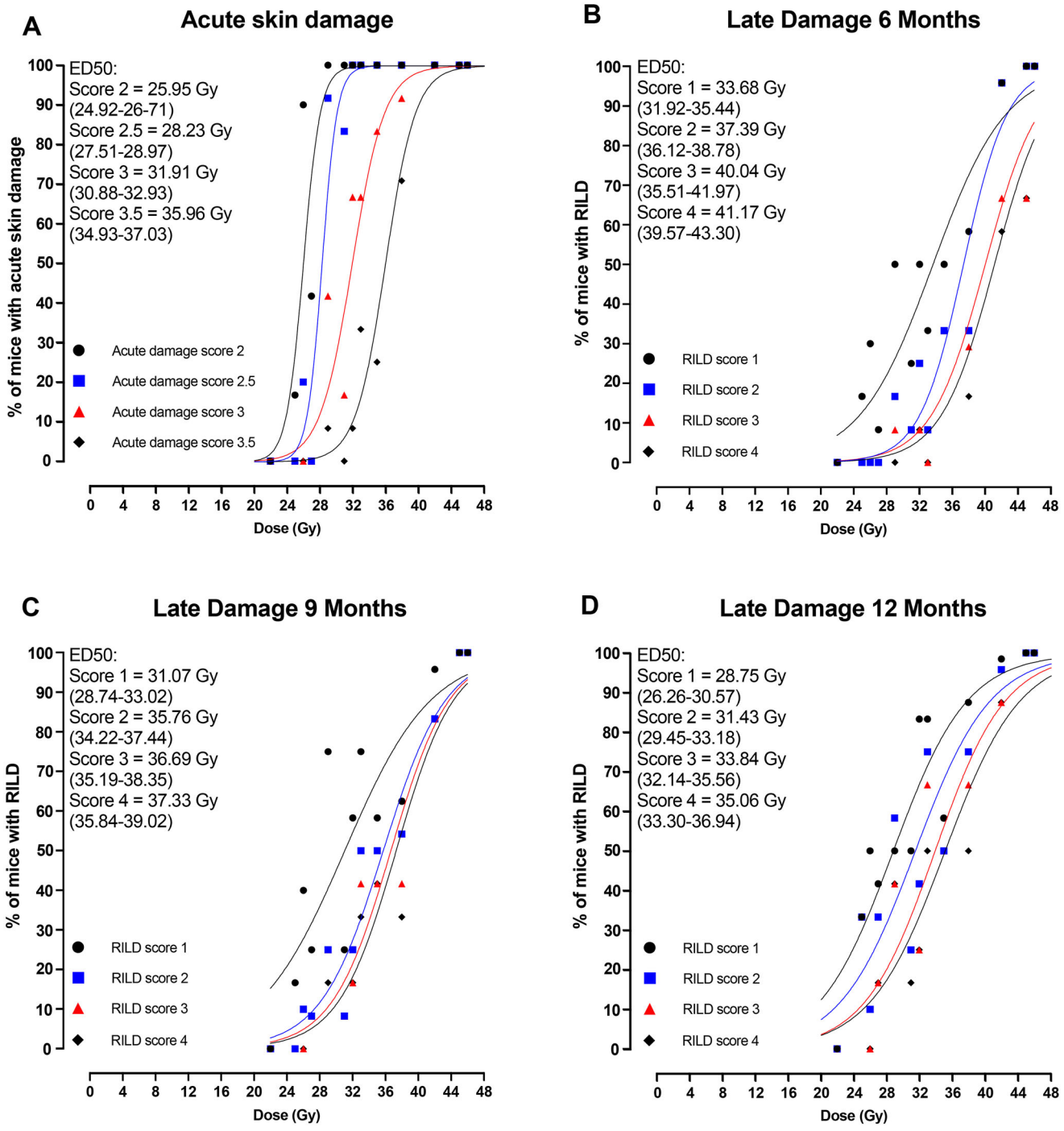


**Figure 2.** Dose–response curves for (A) acute skin damage and late-induced late damage (RILD) after (B) 6 months, (C) 9 months, and (D) 12 months for each end-point severity score where the highest score is the most severe cases. It depicts the percentage of mice (46 Gy, $n = 5$; 22 Gy, 25 Gy, and 45 Gy, $n = 6$; 26 Gy, $n = 10$; 27 Gy, 29 Gy, 31 Gy, 32 Gy, 33 Gy, and 35 Gy, $n = 12$; 38 Gy and 42 Gy, $n = 24$) with acute skin damage or RILD as a function of dose. The ED50 (effective dose at 50% responders) with 95% confidence intervals are indicated on each graph. The symbol punctuation on the curves indicates the percentage of mice with a respective score, and the curves are fitted with simple logistic regression.

is within expectations from the introduction of the thimble-shaped air-filled cavity (the Semiflex IC sensitive volume radius is 2.4 mm, which means a half average cord length of 2*radius/pi = 1.52 mm for parallel beams on cylinders). The plane-parallel Advanced Markus chamber, however, agreed very well with the MC simulations in terms of range, but the measured dose was 1.2% lower than the Semiflex IC measurements in the SOBP. In Figure 4, the results are shown normalized to 100% PTV dose. Geant4 and SHIELD-HIT12A MC seem to be in excellent agreement, in particular in terms of range. Also shown in Figure 4 are the eight mouse leg positions. The average relative dose, LET, and Qeff over these eight positions are summarized in Table 2.

## Discussion

*In vivo* studies are an important step for translating *in vitro* data to clinical standards of care as the living organism's

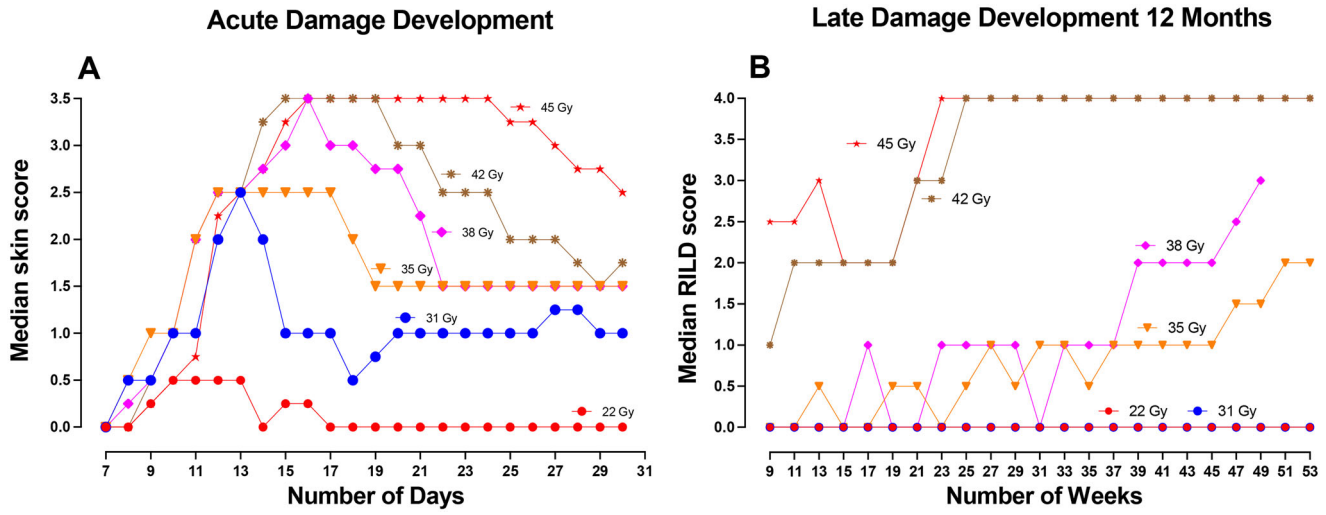


**Figure 3.** Development of endpoints as a function of time. (A) Median skin score on mice feet for each radiation dose as a function of days until day 30 after treatment. (B) The median radiation-induced late damage (RILD) scores for 22 Gy ($n = 6$), 31 Gy and 35 Gy ($n = 12$), 38 Gy and 42 Gy ($n = 24$), and 45 Gy ($n = 6$) were analyzed for 12 months after treatment.

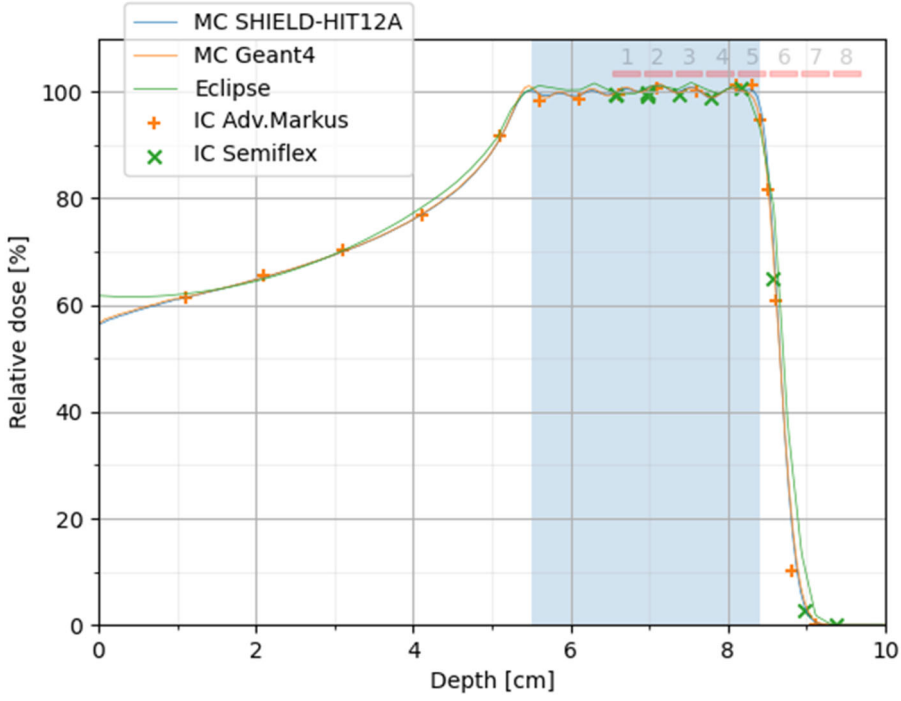


**Figure 4.** Relative dose measurements compared to SHIELD-HIT12A MC simulations. The measurements are based on absolute dose measurements, as described in the results section, but for this plot, the IC data are normalized to 100% PTV dose (by scaling the Semiflex data by 0.8% and Adv. Markus data by 2.0%). Furthermore, the Semiflex data points are displaced by 1.25 mm upstream to compensate for the shift of the effective measurement point introduced by the cylindrical shape of the air-filled cavity. The eight nominal mice positions are shown as red bars over the SOBP and its distal edge.

**Table 2.** SHIELD-HIT12A MC calculated relative dose, dose-averaged LET, and track- and dose-averaged Qeff for the eight nominal mouse leg positions.

| **Position no.** | 1 | 2 | 3 | 4 | 5 | 6 | 7 | 8 |
|---|---|---|---|---|---|---|---|---|
| Depth [cm] | 6.7 | 7.1 | 7.5 | 7.9 | 8.3 | 8.7 | 9.1 | 9.5 |
| Relative mean dose [%] | 99.68 | 100.3 | 100.0 | 99.36 | 98.09 | 43.58 | 1.66 | 0.05 |
| dLET, protons [keV/um] | 3.16 | 3.53 | 3.99 | 4.68 | 6.81 | 11.23 | 15.02 | 9.18 |
| dLET, all [keV/um] | 5.09 | 5.33 | 5.63 | 6.04 | 7.63 | 11.77 | 17.89 | 81.35 |
| dQeff, all [nil] | 136.9 | 138.7 | 139.9 | 141.6 | 163.3 | 260.3 | 474.3 | 3815 |
| tQeff, all [nil] | 17.92 | 20.44 | 23.99 | 30.02 | 47.04 | 89.59 | 141.6 | 118.5 |

Depths are measured from the phantom surface to the center of the corresponding position.

physiology and biology are considered. In this study, we presented a reproducible and transparent radiation setup for *in vivo* investigations using a murine leg model that allows the examination of the biological response of a specific controlled target in a homogenous setting. It enables the assessment of biological responses without the influence of

anesthetics and is feasible to investigate the effects of radiotherapy for both normal tissue toxicity and subcutaneous tumor models. Here, we reported our acute- and late-normal tissue damage categorical assays in detail and presented results from an initiating proton irradiation study covering a year of follow-up from the same mice. The acute skin damage endpoint represents a diagnostic visual analysis of the damaged skin in the targeted area, and the late damage endpoint (RILD) is a more complex endpoint that impairs the functionality of the ankle joint. The loss of functionality in the joint may be caused by commonly observed side effects such as contracture, muscle shortening, atrophy, and predominantly radiation-induced fibrosis [27,29]. This can be investigated histopathologically. The acute skin damage presenting itself on the feet of the mice progresses and heals again during the first month after treatment. RILD, however, slowly progresses in the ankle joint during the year of follow-up, indicating a progressive nature and irreversibility (see Figure 3). Because the isolated radiation target is placed on the extremities, it allows long-term follow-up as the mice bodies (with adequate shielding) are protected against any radiation. As demonstrated in Figure 2, the assays enable us to quantify different degrees of severity in the same mice for both the acute- and late-endpoint in a dose–response relationship. As it is possible to irradiate up to five animals at a time, it enables enough mice to generate full dose–response curves easily with nine or more mice per dose group and reach appropriate narrow confidence intervals for the ED50s and other desired statistical measures [2].

The biological response is influenced by multiple factors. It is sensitive to such as the concentration of oxygen [30–32], temperature [13,19,33], and anesthesia [34–36]. Irradiating a specific target without the use of anesthesia can be exceptionally challenging as the target potential moves, but there has been a lot of discussion on anesthesia and alterations of the radiosensitivity in mice that make it appealing to avoid. In that sense, it also appeals to the logistical and practical challenges in anesthetizing multiple animals, especially when executing multifractionated dose–response studies.

The acute skin damage of the increasing LET toward the proton track end has been investigated for mice irradiated in our setup with a single high dose in eight different positions along the proton SOBP and at the distal dose fall-off [23]. A target that potentially moves is tricky at the dose-depth plane as a few millimeters difference in position affects the physical dose that the mouse foot receives as well as the LET. To overcome this challenge, pictures before and videos during irradiation can monitor the position and movement of the unanesthetized mice, which can be crucial for the result. Nevertheless, it is important to use small targets to investigate the RBE dependency on LET. If larger targets are used, the LET and RBE will be an average estimate of the biological effects. It circumvents averaging the RBE over a large range of increasing LET values, obtaining an adequate spatial resolution across the SOBP. Furthermore, the setup is currently used in proton normal tissue damage and tumor control FLASH studies [37], where mice are irradiated at the entrance of the SOBP to disregard the increased tissue toxicity possible achieved at the distal end. Because of the controlled design and transparency of the setup, it is easy to compare different studies as dose–response curves are easily made.

Full dose–response curves for acute and, especially, late effects are needed to investigate the RBE and other radiation techniques such as FLASH and GRID. Besides proton irradiation, the setup was used for carbon ions to investigate the RBE for normal tissue damage and tumor control [38]. Moreover, with slight modifications, the setup is also used to generate reference curves using photon irradiation. This accentuates the multiradiation modality flexibility the setup offers.

## Conclusion

We here described our experimental radiation setup for *in vivo* biological research, considering the increasing demand for documenting radiobiological setups, radiation response assays, and enclosed details. The presented setup can be used as a template for many radiobiological *in vivo* research purposes, including RBE, FLASH, and GRID, combined with radio-modifying drugs, hypothermia, etc., with only minor alterations. It permits assessment of the same animals' acute- and late-normal tissue toxicities and subcutaneous tumor research. It is feasible for quantifiable cohort sizes to generate full dose–response curves. The flexibility in the positioning of the mice enables research of the varying biological and physical properties at the SOBP entrance, along the SOBP, and at the distal dose fall-off.

## Disclosure statement

No potential conflict of interest was reported by the authors.

## Funding

Supported by the Novo Nordisk Foundation (grant no. NNF195A0059372), DCCC Radiotherapy - The Danish National Research Center for Radiotherapy, Danish Cancer Society (grant no. R167-A10976), INSPIRE (European Union's Horizon 2020 research and innovation program under grant agreement no 730983), A.P. Moller Foundation, and Helga and Peter Korning Foundation.

## ORCID

Fardous Reaz http://orcid.org/0009-0002-8332-9655
Per Poulsen http://orcid.org/0000-0001-9940-7609
Jens Overgaard http://orcid.org/0000-0002-0814-8179
Niels Bassler http://orcid.org/0000-0002-4160-1078
Cai Grau http://orcid.org/0000-0003-3548-3527
Brita Singers Sørensen http://orcid.org/0000-0002-3955-4735

## Data availability statement

The biological raw data is available on request.
Cathrine@oncology.au.dk
The Monte Carlo Simulations are available on:
https://github.com/APTG/2022_DCPT_MICE

A CAD-file outlining the water phantom dimension in detail is provided.

## Acknowledgements

The authors thank Dorthe Grand, Maria Bech, and Marianne Kristiansen for their excellent help in animal care and handling.

## References

[1] Sørensen BS, Overgaard J, Bassler N. In vitro RBE-LET dependence for multiple particle types. Acta Oncol. 2011;50(6):757–762. doi: 10.3109/0284186X.2011.582518.

[2] Paganetti H, Niemierko A, Ancukiewicz M, et al. Relative biological effectiveness (RBE) values for proton beam therapy. Int J Radiat Oncol Biol Phys. 2002;53(2):407–421. doi: 10.1016/s0360-3016(02)02754-2.

[3] Paganetti H. Relative biological effectiveness (RBE) values for proton beam therapy. Variations as a function of biological endpoint, dose, and linear energy transfer. Phys Med Biol. 2014;59(22):R419–R472. doi: 10.1088/0031-9155/59/22/R419.

[4] Sørensen BS. Commentary: RBE in proton therapy–where is the experimental in vivo data? Acta Oncol. 2019;58(10):1337–1339. doi: 10.1080/0284186X.2019.1669819.

[5] Willers H, Allen A, Grosshans D, et al. Toward A variable RBE for proton beam therapy. Radiother Oncol. 2018;128(1):68–75. doi: 10.1016/j.radonc.2018.05.019.

[6] Britten RA, Nazaryan V, Davis LK, et al. Variations in the RBE for cell killing Along the Depth-Dose profile of a modulated proton therapy beam. Radiat Res. 2013;179(1):21–28. doi: 10.1667/RR2737.1.

[7] Chaudhary P, Marshall TI, Perozziello FM, et al. Relative biological effectiveness variation along monoenergetic and modulated bragg peaks of a 62-MeV therapeutic proton beam: a preclinical assessment. Int J Radiat Oncol Biol Phys. 2014;90(1):27–35. doi: 10.1016/j.ijrobp.2014.05.010.

[8] Wouters BG, Skarsgard LD, Gerweck LE, et al. Radiobiological intercomparison of the 160 MeV and 230 MeV proton therapy beams at the harvard cyclotron laboratory and at Massachusetts general hospital. Radiat Res. 2015;183(2):174–187. doi: 10.1667/RR13795.1.

[9] Symonds P, Jones GDD. FLASH radiotherapy: the next technological advance in radiation therapy? Clin Oncol (R Coll Radiol). 2019;31(7):405–406. doi: 10.1016/j.clon.2019.05.011.

[10] Lühr A, von Neubeck C, Pawelke J, et al. "Radiobiology of proton therapy": results of an international expert workshop. Radiother Oncol. 2018;128(1):56–67. doi: 10.1016/j.radonc.2018.05.018.

[11] Henry T, Ureba A, Valdman A, et al. Proton grid therapy: a proof-of-concept study. Technol Cancer Res Treat. 2017;16(6):749–757. doi: 10.1177/1533034616681670.

[12] Wang Y, Deng W, Li N, et al. Combining immunotherapy and radiotherapy for cancer treatment: current challenges and future directions. Front Pharmacol. 2018;9:185. doi: 10.3389/fphar.2018.00185.

[13] Kaur P, Hurwitz MD, Krishnan S, et al. Combined hyperthermia and radiotherapy for the treatment of cancer. Cancers (Basel). 2011;3(4):3799–3823. doi: 10.3390/cancers3043799.

[14] Verhaegen F, Dubois L, Gianolini S, et al. ESTRO ACROP: technology for precision small animal radiotherapy research: optimal use and challenges. Radiother Oncol. 2018;126(3):471–478. doi: 10.1016/j.radonc.2017.11.016.

[15] Ford E, Emery R, Huff D, et al. An image-guided precision proton radiation platform for preclinical in vivo research. Phys Med Biol. 2017;62(1):43–58. doi: 10.1088/1361-6560/62/1/43.

[16] Suckert T, Müller J, Beyreuther E, et al. High-precision image-guided proton irradiation of mouse brain Sub-volumes. Radiother Oncol. 2020;146:205–212. doi: 10.1016/j.radonc.2020.02.023.

[17] Suckert T, Beyreuther E, Müller J, et al. Late side effects in normal mouse brain tissue after proton irradiation. Front Oncol. 2020;10:598360. doi: 10.3389/fonc.2020.598360.

[18] Gueulette J, Slabbert JP, Böhm L, et al. Proton RBE for early intestinal tolerance in mice after fractionated irradiation. Radiother Oncol. 2001;61(2):177–184. doi: 10.1016/s0167-8140(01)00446-7.

[19] Overgaard J. Effect of misonidazole and hyperthermia on the radiosensitivity of a C3H mouse mammary carcinoma and its surrounding normal tissue. Br J Cancer. 1980;41(1):10–21. doi: 10.1038/bjc.1980.2.

[20] Pedersen KH, Kunugi KA, Hammer CG, et al. Radiation biology irradiator dose verification survey. Radiat Res. 2016;185(2):163–168. doi: 10.1667/RR14155.1.

[21] Desrosiers M, DeWerd L, Deye J, et al. The importance of dosimetry standardization in radiobiology. J Res Natl Inst Stand Technol. 2013;118:403.

[22] Koontz BF, Verhaegen F, Ruysscher DDE. Tumour and normal tissue radiobiology in mouse models : how close are mice to mini-humans ? Br J Radiol. 2017;90:1–7.

[23] Singers Sørensen B, Bassler N, Nielsen S, et al. Relative biological effectiveness (RBE) and distal edge effects of proton radiation on early damage in vivo. Acta Oncol. 2017;56(11):1387–1391. doi: 10.1080/0284186X.2017.1351621.

[24] Mather SJ, Mansi L. IAEA technical report series. Eur J Nucl Med Mol Imaging. 2008;35(5):1030–1031. doi: 10.1007/s00259-008-0767-4.

[25] Palmans H, Lourenço A, Medin J, et al. Current best estimates of beam quality correction factors for reference dosimetry of clinical proton beams. Phys Med Biol. 2022;67:195012. doi: 10.1088/1361-6560/ac9172.

[26] Von der Maase H. Effect of cancer chemotherapeutic drugs on the radiation-induced skin reactions in mouse feet. Br J Radiol. 1984;57(680):697–707. doi: 10.1259/0007-1285-57-680-697.

[27] Stone HB. Leg contracture in mice: an assay of normal tissue response. Int J Radiat Oncol Biol Phys. 1984;10(7):1053–1061. doi: 10.1016/0360-3016(84)90177-9.

[28] Nawroth I, Alsner J, Behlke MA, et al. Intraperitoneal administration of chitosan/DsiRNA nanoparticles targeting TNFα prevents radiation-induced fibrosis. Radiother Oncol. 2010;97(1):143–148. doi: 10.1016/j.radonc.2010.09.010.

[29] Straub JM, New J, Hamilton CD, et al. Radiation-induced fibrosis: mechanisms and implications for therapy. Radiation-Induced Fibros Mech Implic Ther. 2016;141:1–16.

[30] Rockwell S, Dobrucki I, Kim E, et al. Hypoxia and radiation therapy: past history, ongoing research, and future promise. Curr Mol Med. 2009;9(4):442–458. doi: 10.2174/156652409788167087.

[31] Overgaard J. Hypoxic radiosensitization: adored and ignored. J Clin Oncol. 2007;25(26):4066–4074. doi: 10.1200/JCO.2007.12.7878.

[32] Churchill-Davidson I. Oxygen effect on radiosensitivity. Cancer. 1960;13(S6):122–132. doi: 10.1002/1097-0142(196011/12)13:6+<122::AID-CNCR2820130719>3.0.CO;2-Q.

[33] Elming PB, Sørensen BS, Oei AL, et al. Hyperthermia: the optimal treatment to overcome radiation resistant hypoxia. Cancers (Basel). 2019;11(1):60. doi: 10.3390/cancers11010060.

[34] Merriam G, Focht E, Parsons W, et al. Influence of anesthesia on radiation effect. Radiology 1968;91(4):694–697. doi: 10.1148/91.4.694.

[35] Suit HD, Sedlacek RS, Silver G, et al. Pentobarbital anesthesia and the response of tumor and normal tissue in the C3Hf/sed mouse to radiation. Radiat Res. 1985;104(1):47–65. doi: 10.2307/3576776.

[36] Wondergem J, Haveman J, Van Der Schueren E, et al. The influence of misonidazole on the radiation response of murine tumors of different size: possible artifacts caused by pentobarbital sodium anesthesia. Int J Radiat Oncol Biol Phys. 1981;7(6):755–760. doi: 10.1016/0360-3016(81)90469-7.

[37] Singers Sørensen B, Krzysztof Sitarz M, Ankjærgaard C, et al. In vivo validation and tissue sparing factor for acute damage of pencil beam scanning proton FLASH. Radiother Oncol. 2022;167:109–115. doi: 10.1016/j.radonc.2021.12.022.

[38] Sørensen BS, Horsman MR, Alsner J, et al. Relative biological effectiveness of carbon ions for tumor control, acute skin damage and late radiation-induced fibrosis in a mouse model. Acta Oncol. 2015;54(9):1623–1630. doi: 10.3109/0284186X.2015.1069890.